PCCP

Cite this: *Phys. Chem. Chem. Phys.*, 2012, **14**, 1412–1417

www.rsc.org/pccp

PAPER

Butylphenyl-functionalized Pt nanoparticles as CO-resistant electrocatalysts for formic acid oxidation

Zhi-You Zhou,[ab] Jie Ren,[b] Xiongwu Kang,[a] Yang Song,[a] Shi-Gang Sun[b] and Shaowei Chen*[a]

Received 7th October 2011, Accepted 17th November 2011
DOI: 10.1039/c1cp23183a

Butylphenyl-functionalized Pt nanoparticles (Pt-BP) with an average core diameter of 2.93 ± 0.49 nm were synthesized by the co-reduction of butylphenyl diazonium salt and H_2PtCl_4. Cyclic voltammetric studies of the Pt-BP nanoparticles showed a much less pronounced hysteresis between the oxidation currents of formic acid in the forward and reverse scans, as compared to that on naked Pt surfaces. Electrochemical *in situ* FTIR studies confirmed that no adsorbed CO, a poisoning intermediate, was generated on the Pt-BP nanoparticle surface. These results suggest that functionalization of the Pt nanoparticles by butylphenyl fragments effectively blocked the CO poisoning pathway, most probably through third-body effects, and hence led to an apparent improvement of the electrocatalytic activity in formic acid oxidation.

1. Introduction

Direct formic acid fuel cell (DFAFC) is a promising power source for portable electronic devices. In comparison with its analogues (*e.g.*, direct methanol fuel cell), DFAFC has the merits such as fast kinetics of formic acid electrooxidation, low toxicity of formic acid, as well as low crossover rates of formic acid through Nafion membranes.[1,2] The crossover of fuels from anode to cathode will result in the loss of fuels and the "mixed potential" that decreases the efficiency of oxygen reduction. The main challenge of DFAFC is that the anode electrocatalysts can be easily poisoned by CO. It is well established that the electrooxidation of formic acid on Pt is *via* a dual-path mechanism that involves reactive intermediates and poisoning intermediates.[3] The chemical nature of the active intermediates is still under dispute, and adsorbed formate ions have been proposed as a possible form.[3–6] The poisoning intermediates are mainly adsorbed CO (CO_{ad}) species, which are formed through spontaneously dissociative adsorption (*i.e.*, dehydration) of HCOOH.[3] CO_{ad} is difficult to remove unless at a potential (*e.g.*, +0.6 V *vs.* RHE) far exceeding the working potential in DFAFC. Therefore, Pt catalysts can be easily self-poisoned by CO_{ad} during formic acid electrooxidation. Clearly, the suppression of the CO pathway is key to the improvement of the catalytic performance of Pt electrodes for formic acid oxidation.

Generally, increasing the CO resistance of Pt catalysts for formic acid oxidation relies on chemical modification of the Pt surfaces with foreign metal atoms (such as Bi, Pb, and Sb).[7–10] These foreign atoms provide steric hindrance for formic acid to form CO_{ad}, *i.e.*, the so-called third-body effects.[11,12] In some other studies, macrocycle molecules (*e.g.*, iron–tetrasulfophthalocyanine) have also been found to inhibit self-poisoning of Pt in formic acid oxidation, as demonstrated by Xing and coworkers.[13,14]

Recently, surface functionalization of noble metal nanoparticles with aryl groups through diazonium salts has received increasing attention.[15–23] This may yield new and promising catalysts for fuel cell electrochemistry. For example, we have synthesized butylphenyl-functionalized Pd nanoparticles (Pd-BP) by virtue of the palladium–carbon covalent linkages.[21] Because of the small core size (2.24 nm) and very high specific electrochemical surface area (122 $m^2\ g^{-1}_{Pd}$), the Pd-BP nanoparticles exhibited a mass activity ~4.5 times that of commercial Pd black for HCOOH electrooxidation.

Herein, by using a similar method, we prepared butylphenyl-stabilized platinum (Pt-BP) nanoparticles (core dia. 2.93 ± 0.49 nm). Cyclic voltammetric and electrochemical *in situ* FTIR spectroscopic measurements demonstrated that the functionalization of the Pt nanoparticle surface by butylphenyl fragments effectively blocked the CO poisoning pathway. As a result, the Pt-BP nanoparticles exhibited much enhanced electrocatalytic activity over commercial Pt/C catalysts towards formic acid electrooxidation.

2. Experimental section

2.1 Synthesis of Pt-BP nanoparticles

The Pt-BP nanoparticles were synthesized by the co-reduction of H_2PtCl_4 and butylphenyldiazonium. The procedure was

[a] *Department of Chemistry and Biochemistry, University of California, 1156 High Street, Santa Cruz, California 95064, USA. E-mail: shaowei@ucsc.edu*
[b] *State Key Laboratory of Physical Chemistry of Solid Surfaces, Department of Chemistry, College of Chemistry and Chemical Engineering, Xiamen University, Xiamen, Fujian 361005, China*

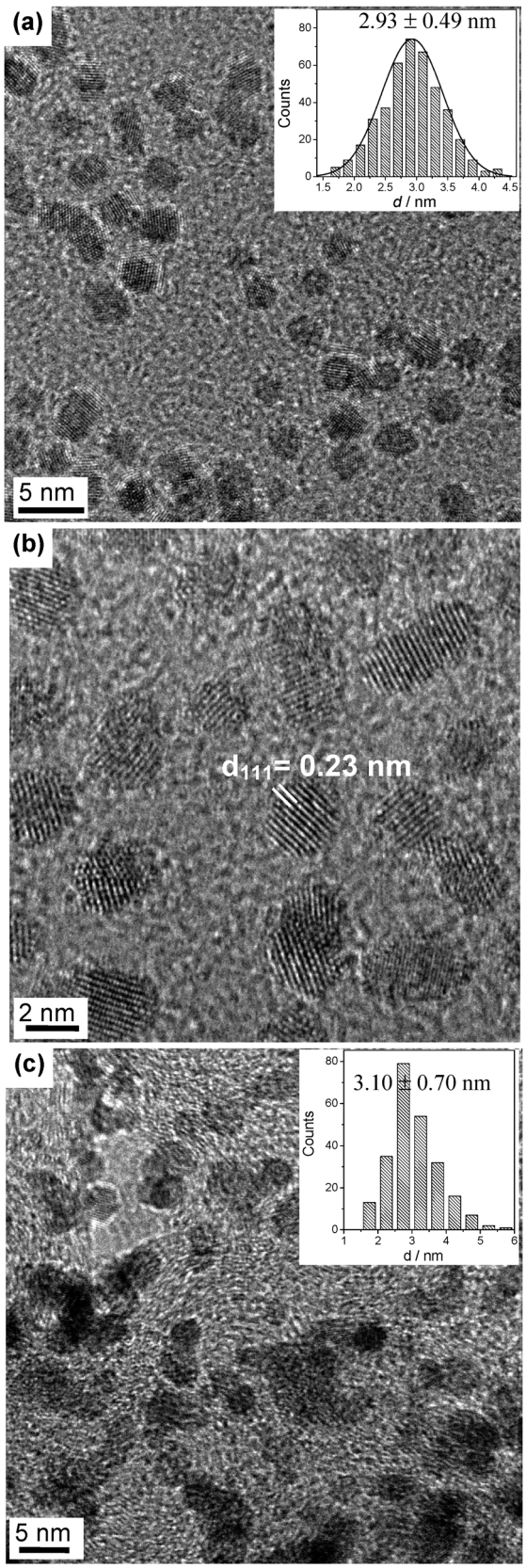

Fig. 1 TEM images of Pt-BP nanoparticles (a, b) and commercial Pt/C catalysts (c). Insets depict the corresponding core size histograms. White lines in (b) highlight the Pt(111) lattice fringes.

similar to that used for the synthesis of butylphenyl-stabilized palladium nanoparticles that we reported previously.[21] Briefly, the diazonium salt was synthesized from a stoichiometric amount of 4-butylaniline (1 mmol) and sodium nitrite in ice-cold 50 wt% fluoroboric acid. H_2PtCl_4 was prepared by dissolving $PtCl_2$ (0.1 mmol) into hydrochloric acid under heating. Both the diazonium salt and H_2PtCl_4 were then added into a toluene–THF (1 : 1 v/v) mixed solvent, and co-reduced by $NaBH_4$ to form a dark-brown solution containing Pt-BP nanoparticles. Subsequently, the solution was washed with 0.1 M H_2SO_4 solution and water several times. After most of the solvent was removed by a rotary evaporator, the Pt-BP nanoparticles were precipitated by ethanol, which were then collected by centrifugation and further washed four times with dichloromethane–ethanol (v : v 1 : 8) to remove impurities and excessive free ligands. Finally, the purified Pt nanoparticles were dissolved in dichloromethane.

2.2 Characterization and electrocatalytic tests of Pt-BP nanoparticles

The morphology of the Pt-BP nanoparticles was characterized by high-resolution transmission electron microscopy (HRTEM, Philips CM300 at 300 kV). The surface ligands were characterized by infrared spectroscopy (Perkin-Elmer Spectrum One FTIR Spectrometer). The IR samples were prepared by drop-casting a concentrated solution of Pt-BP in dichloromethane onto a NaCl disk under a dry N_2 atmosphere. After solvent evaporation, a uniform thin film of nanoparticles was formed. The surface coverage of the organic ligands was measured by thermogravimetric analysis (TGA, Perkin-Elmer Pyris 1) under high-purity N_2 at a heating rate of 10 °C min^{-1}.

Electrochemical tests were carried out in a standard three-electrode cell connected to a CHI 440 electrochemical workstation, with a Pt foil counter electrode and a saturated calomel electrode (SCE) at room temperature. To prepare the working electrode, a calculated amount of Pt-BP nanoparticle solution was dropcast onto a polished glassy carbon (GC, ϕ = 5 mm) electrode. As soon as the nanoparticles were dried in air, the electrode was washed with ethanol, and then dried in N_2. Finally, a dilute Nafion solution (0.1 wt%, 2 μL) was added onto it. A commercial Pt/C catalyst (E-TEK, 30 wt% Pt) was also loaded onto the GC electrode in a similar fashion and employed as a benchmark material to compare the electrocatalytic activity of Pt-BP nanoparticles for formic acid oxidation. The mass loading of Pt on the GC electrode was 0.80 μg in both cases.

The electrocatalytic activity was tested in 0.1 M H_2SO_4 + 0.1 M HCOOH at room temperature by cyclic voltammetry. The experimental details of electrochemical *in situ* FTIR measurement have been described previously.[24] A thin-layer IR cell with a CaF_2 planar window was employed to reduce the intensive IR absorption by water.

3. Results and discussion

3.1 TEM characterization

Fig. 1(a) shows a representative TEM image of the as-prepared Pt-BP nanoparticles. The nanoparticles are well dispersed, suggesting effective passivation by the butylphenyl fragments, thanks

to the formation of Pt–C covalent bonds. Well-defined lattice fringes with a spacing of 0.23 nm, corresponding to the (111) lattice spacing of Pt, can be observed clearly in the HRTEM measurements (Fig. 1(b)). The average core size of Pt-BP nanoparticles was determined to be 2.93 ± 0.49 nm by statistical analysis of over 400 nanoparticles (inset to panel (a)). This size is slightly smaller than that of the commercial Pt/C catalysts used in this study (panel (c)) which exhibited an average core diameter of 3.10 ± 0.70 nm.

3.2 Infrared spectroscopic and TGA characterizations of Pt-BP nanoparticles

Fig. 2(a) depicts the transmission IR spectrum of Pt-BP nanoparticles. The band at 3029 cm^{-1} can be assigned to the stretching vibration of C–H on the phenyl ring, and the three bands at 2955, 2929, 2858 cm^{-1} may be assigned to the saturated C–H stretches of the butyl group. The aromatic ring skeleton vibration can be identified by a very strong band at 1577 cm^{-1}. In addition, the weak band at 827 cm^{-1} is the characteristic peak of the *para*-substituted aromatic ring (out-of-plane C–H deformation vibration). These infrared characteristics demonstrate that butylphenyl fragments have indeed been linked to the Pt surface successfully.

The amount of organic ligands on the Pt-BP nanoparticles was determined by thermogravimetric analysis (Fig. 2(b)) to be about 27%. The rapid mass loss occurred at about 300 °C. On the basis of the weight loss and the average core size (2.93 nm) of the Pt nanoparticles, we can estimate that the average area occupied by one butylphenyl ligand on the Pt nanoparticle surface is about 5.8 $Å^2$. This value is consistent with that of decylphenyl-stabilized Pt nanoparticles (~5.5 $Å^2$) reported previously,[15] but considerably lower than the typical value (~20 $Å^2$) for long-chain alkanethiolates adsorbed on metal nanoparticles.[25] Such a small footprint suggests the formation of some multilayer polyaryl structure on the Pt surfaces.[26,27]

3.3 Electrocatalytic tests for HCOOH oxidation

Fig. 3(a) shows the cyclic voltammograms of Pt-BP nanoparticles (solid curve) and commercial Pt/C (dashed curve) catalysts in 0.1 M H_2SO_4 solution at a potential sweep rate of 100 mV s^{-1}. The currents were normalized to the mass loading of Pt on the electrode surfaces. On the Pt/C modified electrode, two pairs of current peaks can be observed clearly within the potential range of 0 to −0.2 V. These are ascribed to hydrogen adsorption and desorption on Pt surfaces. In contrast, on the Pt-BP modified electrode, the current peaks of hydrogen adsorption and desorption are very broad and not well-defined. Furthermore, the current density is considerablly lower than that of Pt/C, although the Pt-BP nanoparticles have smaller core size (Fig. 1). This discrepancy may be attributable to the blocking of some Pt surface sites by the butylphenyl fragments on the Pt-BP nanoparticle surface. Based on the charge of hydrogen adsorption/desorption, the specific electrochemical surface areas (ECSA) of the Pt-BP and Pt/C electrodes are determined to be 21 and 54 $m^2\ g^{-1}_{Pt}$, respectively. The theoretical ECSA of Pt-BP nanoparticles (dia. 2.93 nm) was estimated to be 95 $m^2\ g^{-1}$, suggesting that only about 22% of the particle surface was electrochemically accessible.

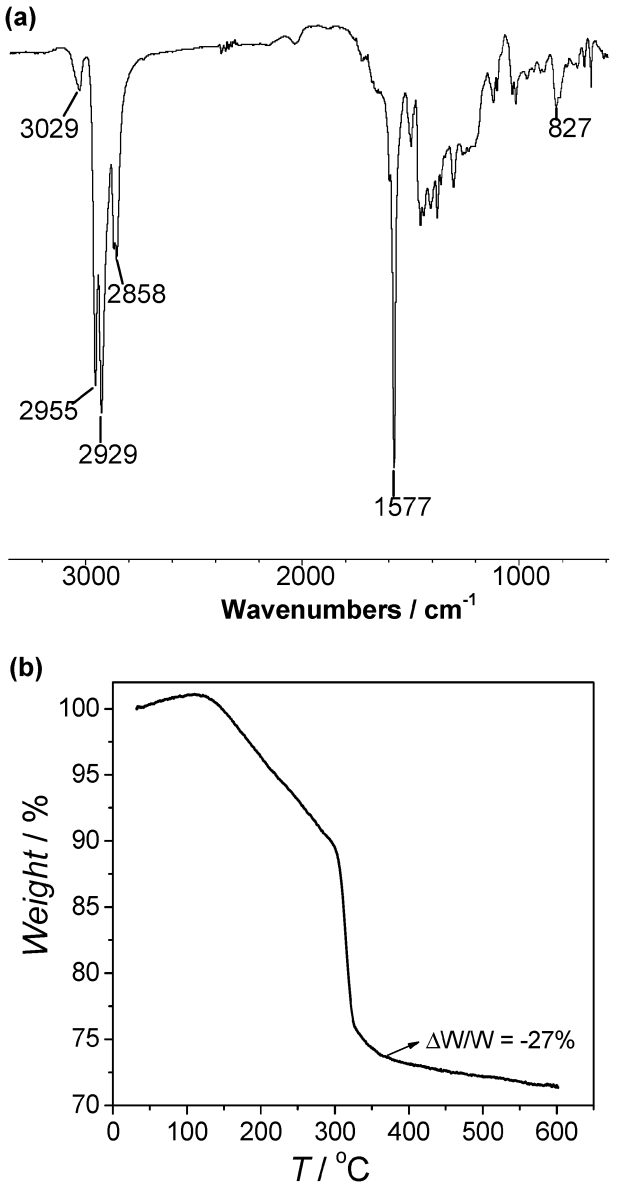

Fig. 2 (a) Transmission FTIR spectrum of Pt-BP nanoparticles. (b) TGA curve of Pt-BP nanoparticles measured under a N_2 atmosphere at a heating rate of 10 °C min^{-1}.

The most interesting property of the Pt-BP nanoparticles is that surface functionalization by the butylphenyl groups led to drastic suppression of CO poisoning in formic acid electrooxidation. Fig. 3(b) compares the cyclic voltammograms of Pt-BP (solid curve) and commercial Pt/C (dashed curve) catalysts recorded in a 0.1 M HCOOH + 0.1 M H_2SO_4 solution at a potential sweep rate of 50 mV s^{-1}. On the Pt/C electrode, along with increasing electrode potential, a weak and broad oxidation peak appears at around +0.30 V, followed by a sharp peak at +0.60 V in the forward scan. The former is attributed to the direct oxidation of formic acid to CO_2 on surface catalytic sites that were not occupied by CO species, while the latter is assigned to the oxidation of CO_{ad} that is generated from the spontaneous dissociative adsorption of formic acid on Pt surfaces.[28] After the oxidative stripping of CO_{ad} species, formic acid can be readily oxidized on the clean Pt surface, as indicated by a very intensive

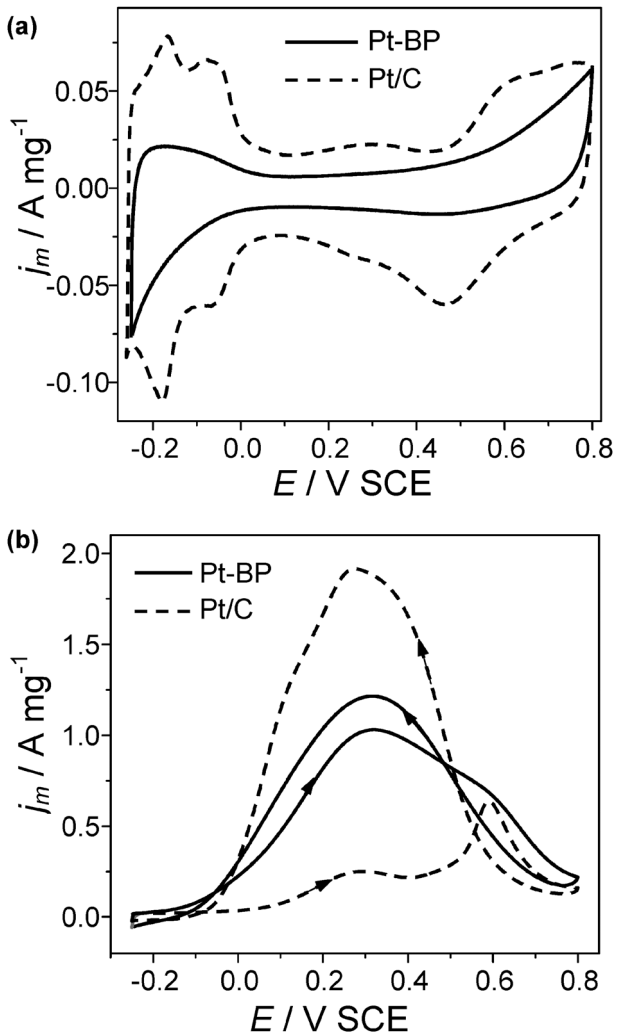

Fig. 3 Cyclic voltammograms of Pt-BP nanoparticles and commercial Pt/C catalyst in (a) 0.1 M H_2SO_4 and (b) 0.1 M HCOOH + 0.1 M H_2SO_4. The currents were all normalized by the mass loading of Pt. Potential scan rate was 100 mV s^{-1} in (a), and 50 mV s^{-1} in (b).

current peak at *ca.* +0.3 V in the reverse scan. In contrast, on the Pt-BP nanoparticles, the hysteresis between the oxidation currents of formic acid in the forward and reverse scans is much less pronounced, and only a small hump can be observed in the same potential region (~ +0.60 V) for CO_{ad} oxidation in the forward scan. This fact indicates that the CO poisoning pathway has been greatly suppressed on the Pt-BP nanoparticle surface. As a result, the peak current density of formic acid oxidation on the Pt-BP electrode (1.03 A mg$^{-1}_{Pt}$) is about 4 times larger than that on the Pt/C electrode (0.25 A mg$^{-1}_{Pt}$) in the forward scan at around +0.30 V. However, in the reverse scan after CO stripping, Pt/C (1.92 A mg$^{-1}_{Pt}$) shows a larger current density than Pt-BP (1.22 A mg$^{-1}_{Pt}$), which is most likely due to the occupation of part of the Pt surface sites by the butylphenyl ligands, *i.e.*, less free surface sites accessible for formic acid oxidation, as compared to the "bare" Pt/C catalysts.

When the current of formic acid oxidation was normalized to free Pt surfaces (*i.e.*, ECSA), the enhancement factor of the catalytic activity for Pt-BP over Pt/C is 10.6 and 1.6 in the forward and reverse scans, respectively. The latter is similar to

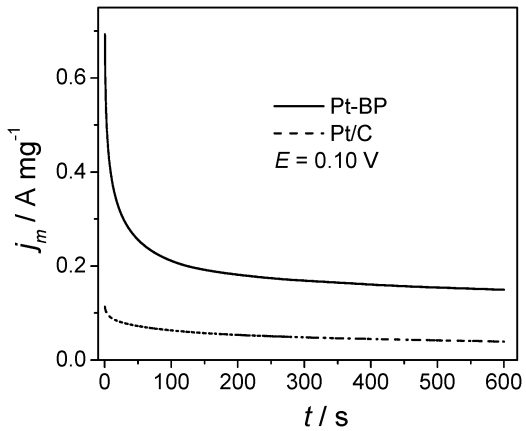

Fig. 4 Current–time curves recorded at 0.10 V of HCOOH oxidation on Pt-BP (solid line) and commercial Pt/C (dashed line) catalysts in 0.1 M HCOOH + 0.1 M H_2SO_4.

that (1.3) observed with Pd-BP for formic acid oxidation that was reported previously,[21] indicating that the enhancement by butylphenyl modification for Pt and Pd catalysts is comparable. Therefore, the improved activity of the Pt-BP nanoparticles is most likely attributed to 'anti-CO' poisoning, and less likely to other factors such as electronic effects.

We also acquired the current–time curves of formic acid oxidation at +0.10 V (close to the working potential of direct formic acid fuel cells) to evaluate the stability of the catalysts. As shown in Fig. 4, Pt-BP (solid curve) showed a very high initial activity, but it degraded quickly, and reached a steady state after 100 s. Nevertheless, at 600 s, the steade-state current density of Pt-BP (0.154 A mg^{-1}) was still about 4 times that of Pt/C (0.039 A mg^{-1}, dashed curve). This result indicates that although Pt-BP nanoparticles show a relatively high degradation rate, they can still provide much higher stead-state currents than commerical Pt/C.

3.4 *In situ* FTIR studies of formic acid electrooxidation

The suppression of CO poisoning for formic acid oxidation on the Pt-BP nanoparticles was further confirmed by electrochemical *in situ* FTIR spectroscopic measurements. Fig. 5 shows the FTIR spectra of formic acid electrooxidation on the (a) Pt-BP and (b) commercial Pt/C catalysts at potentials ranging from −0.20 to +0.10 V at an interval of 0.05 V. The reference spectra were acquired at −0.25 V, where the oxidation of formic acid and dissociative adsorption of formic acid to form CO_{ad} were negligible. In Fig. 5, the downward bands at 2343 cm^{-1} were assigned to CO_2, the oxidation product of formic acid; the band at around 2050 cm^{-1} in the spectra of the Pt/C electrode (panel (b)) is attributed to linearly bonded CO (CO_L), a poisoning intermediate species of formic acid oxidation. In sharp contrast, the production of adsorbed CO is negligible on the Pt-BP surface (panel (a)), confirming that the functionalization of Pt nanoparticles by the butylphenyl fragments has effectively blocked the poisoning pathway of formic acid oxidation. As a result, more CO_2 was produced on Pt-BP than on Pt/C at the same potentials.

It has been known that there are at least two factors that are responsible for the improved performance of electrocatalysts

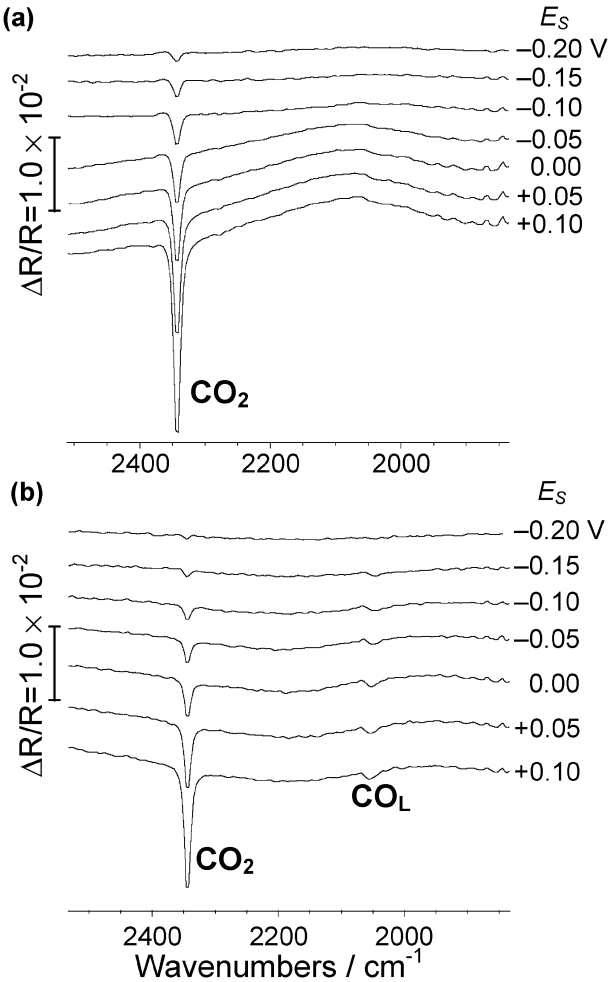

Fig. 5 Electrochemical *in situ* FTIR spectra of formic acid oxidation on the (a) Pt-BP nanoparticles and (b) commercial Pt/C catalyst in 0.1 M HCOOH + 0.1 M H_2SO_4 at different potentials (E_S), which was varied from −0.20 to +0.10 V, with the reference spectra acquired at E_R = −0.25 V.

for formic acid oxidation: third-body effects (or geometric effects) and electronic structure effects.[12,29] As for third-body effects, it is generally accepted that the dehydration of formic acid to form CO_{ad} is a site demanding reaction, where several neighboring Pt sites are required.[12] This pathway may be blocked if the Pt surfaces are covered by some foreign atoms (*e.g.*, Pb and Bi atoms) or organic surface ligands. Therefore, within the present experimental context, the high catalytic activity of the Pt-BP nanoparticles observed above (Fig. 3) may be, at least in part, attributed to this third-body effect. That is, the surface-bound butylphenyl fragments result in steric hindrance for the formation of CO_{ad} from formic acid. Certainly, the contributions of the electronic effects cannot be excluded at this point. Further studies are desired to unravel the fundamental mechanism of surface chemical functionalization in the manipulation and improvement of nanoparticle electrocatalytic activity.

4. Conclusions

In summary, we have synthesized stable butylphenyl-functionalized platinum (Pt-BP) nanoparticles. Both cyclic voltammetric and electrochemical *in situ* FTIR spectroscopic results demonstrated that the CO poisoning pathway of formic acid electrooxidation had been greatly suppressed on the Pt-BP surface, most probably because of the unique surface-functionalization that sterically hindered the formation of adsorbed CO from formic acid. As a result, the Pt-BP nanoparticles exhibited markedly higher catalytic activity than commercial Pt/C for formic acid electrooxidation. The present study demonstrates that surface functionalization of noble metal nanoparticles may be a promising route towards the improvement of the catalytic performance of fuel cell electrocatalysts.

Acknowledgements

This work was supported by the National Science Foundation (CHE-1012258), the ACS-Petroleum Research Fund (49137-ND10), and National Natural Science Foundation of China (21073152). TEM studies were carried out at the National Center for Electron Microscopy, Lawrence Berkeley National Laboratory, which is supported by the US Department of Energy.

References

1 X. W. Yu and P. G. Pickup, *J. Power Sources*, 2008, **182**, 124.
2 Y. W. Rhee, S. Y. Ha and R. I. Masel, *J. Power Sources*, 2003, **117**, 35.
3 S. G. Sun, J. Clavilier and A. Bewick, *J. Electroanal. Chem.*, 1988, **240**, 147.
4 Y. X. Chen, M. Heinen, Z. Jusys and R. J. Behm, *Angew. Chem., Int. Ed.*, 2006, **45**, 981.
5 M. Osawa, K. Komatsu, G. Samjeske, T. Uchida, T. Ikeshoji, A. Cuesta and C. Gutierrez, *Angew. Chem., Int. Ed.*, 2011, **50**, 1159.
6 W. Gao, J. A. Keith, J. Anton and T. Jacob, *J. Am. Chem. Soc.*, 2010, **132**, 18377.
7 M. Watanabe, M. Horiuchi and S. Motoo, *J. Electroanal. Chem.*, 1988, **250**, 117.
8 B. Peng, H. F. Wang, Z. P. Liu and W. B. Cai, *J. Phys. Chem. C*, 2010, **114**, 3102.
9 Q. S. Chen, Z. Y. Zhou, F. J. Vidal-Iglesias, J. Solla-Gullon, J. M. Feliu and S. G. Sun, *J. Am. Chem. Soc.*, 2011, **133**, 12930.
10 A. Lopez-Cudero, F. J. Vidal-Iglesias, J. Solla-Gullon, E. Herrero, A. Aldaz and J. M. Feliu, *J. Electroanal. Chem.*, 2009, **637**, 63.
11 E. Herrero, J. M. Feliu and A. Aldaz, *J. Electroanal. Chem.*, 1994, **368**, 101.
12 E. Leiva, T. Iwasita, E. Herrero and J. M. Feliu, *Langmuir*, 1997, **13**, 6287.
13 Z. G. Zhang, X. C. Zhou, C. P. Liu and W. Xing, *Electrochem. Commun.*, 2008, **10**, 131.
14 X. C. Zhou, W. Xing, C. P. Liu and T. H. Lu, *Electrochem. Commun.*, 2007, **9**, 1469.
15 F. Mirkhalaf, J. Paprotny and D. J. Schiffrin, *J. Am. Chem. Soc.*, 2006, **128**, 7400.
16 D. Ghosh and S. W. Chen, *J. Mater. Chem.*, 2008, **18**, 755.
17 V. K. R. Kumar and K. R. Gopidas, *Chem.–Asian J.*, 2010, **5**, 887.
18 F. Mirkhalaf and D. J. Schiffrin, *Langmuir*, 2010, **26**, 14995.
19 G. Z. Liu, E. Luais and J. J. Gooding, *Langmuir*, 2011, **27**, 4176.
20 V. K. R. Kumar and K. R. Gopidas, *Tetrahedron Lett.*, 2011, **52**, 3102.
21 Z. Y. Zhou, X. W. Kang, Y. Song and S. W. Chen, *Chem. Commun.*, 2011, **47**, 6075.
22 D. E. Jiang, B. G. Sumpter and S. Dai, *J. Am. Chem. Soc.*, 2006, **128**, 6030.

23 L. Laurentius, S. R. Stoyanov, S. Gusarov, A. Kovalenko, R. B. Du, G. P. Lopinski and M. T. McDermott, *ACS Nano*, 2011, **5**, 4219.
24 S. G. Sun and Y. Lin, *Electrochim. Acta*, 1998, **44**, 1153.
25 M. J. Hostetler, J. E. Wingate, C. J. Zhong, J. E. Harris, R. W. Vachet, M. R. Clark, J. D. Londono, S. J. Green, J. J. Stokes, G. D. Wignall, G. L. Glish, M. D. Porter, N. D. Evans and R. W. Murray, *Langmuir*, 1998, **14**, 17.
26 A. Adenier, C. Combellas, F. Kanoufi, J. Pinson and F. I. Podvorica, *Chem. Mater.*, 2006, **18**, 2021.
27 J. K. Kariuki and M. T. McDermott, *Langmuir*, 1999, **15**, 6534.
28 A. Capon and R. Parsons, *J. Electroanal. Chem.*, 1973, **45**, 205.
29 X. H. Xia and T. Iwasita, *J. Electrochem. Soc.*, 1993, **140**, 2559.